Organic Electronics 13 (2012) 1443–1455

Contents lists available at SciVerse ScienceDirect

Organic Electronics

journal homepage: www.elsevier.com/locate/orgel

Photocrosslinkable liquid–crystalline polymers for stable photovoltaics by adjusting side-chains spacing and fullerene size to control intercalation

Kai Yao [a,1], Lie Chen [a,b,1], Ting Hu [a,b], Yiwang Chen [a,b,*]

[a] Institute of Polymers/Department of Chemistry, Nanchang University, 999 Xuefu Avenue, Nanchang 330031, China
[b] Jiangxi Provincial Key Laboratory of New Energy Chemistry, Nanchang University, 999 Xuefu Avenue, Nanchang 330031, China

ARTICLE INFO

Article history:
Received 17 February 2012
Received in revised form 19 March 2012
Accepted 23 March 2012
Available online 19 April 2012

Keywords:
Photovoltaics
Liquid crystals
Conjugated polymers
Photo-crosslink

ABSTRACT

We report a novel copolymer system with high crystallinity and photocrosslinkable building blocks for π–π intermolecular interactions that is, an alternating copolymer with liquid–crystalline nature, and heat/solvent resistance. By copolymerization of 2,5-bis(3-bromododecylthiophen-2-yl)thieno[3,2-b]thiophene (BbTTT) monomer with thiophene and thieno[3,2-b]thiophene via Stille reaction, two novel copolymers PBbTTT-T and PBbTTT-TT have been synthesized. The balanced space between fullerene size and the side-chains of the polymer is crucial to determine the optimum polymer:fullerene blending ratios and the formation of intercalated nanostructure, in which the lamellar arrangement can be controlled by adjusting the fullerene size. This pre-optimum bimolecular crystal morphology can be frozen and preserved with long term performance after UV treatment, a clear advantage for the photo-crosslinking strategy. Furthermore, the free space in the intercalation impacts greatly on the stability of the donor–acceptor bicontinuous network, especially after photocrosslinking. The bulk-heterojunction organic photovoltaics based on PBbTTT-TT:$PC_{71}BM$ at 1:3.5 by weight shows an stable, well-ordered and intercalated nanostructure with an efficiency higher than 2.4% after 40 h annealing at an elevated temperature of 150 °C.

1. Introduction

The growing interests in polymer solar cells (PSCs) [1] are related to their unique advantages such as low-cost manufacturing and easy processability over large-area size [2], which enable them for potential applications in low-cost photovoltaic systems. Although the power conversion efficiency (PCE) of state-of-the-art PSCs has already exceeded 8% in scientific literature [3], further improvements are needed for mass production and practical applications. And for most combinations of material, there are no design rules to predict when the fullerene will mix with the polymer on the molecular scale and when large-scale phase separation will occur; despite the importance that mixing has on exciton harvesting and charge recombination.

In a bulk-heterojunction (BHJ), the efficiency of charge transfer from donor to acceptor can be unity as the donor–acceptor are often phase separated at the length scale within the exciton diffusion length (10–20 nm) [4]. Therefore control of the nanoscale morphology or microstructure of the blend is critical to ensuring that all excitons are collected and dissociated. Once the exciton has dissociated, the free holes and electrons must then be transported through the donor and acceptor phases to their respective electrodes. Within each phase, molecular ordering and, in particular, π–π stacking is important for efficient exciton and charge transport, and in addition usually assists in the absorption of long wavelength light [5]. Hence, polymers with a high tendency to crystallize are preferred and specific arrangement of molecules within the film can be controlled. Poly(2,5-bis(3-alkylthiophen-2-yl)thieno[3,2-b]thiophene)

* Corresponding author at: Institute of Polymers/Department of Chemistry, Nanchang University, 999 Xuefu Avenue, Nanchang 330031, China. Tel.: +86 791 83969562; fax: +86 791 83969561.
E-mail address: ywchen@ncu.edu.cn (Y. Chen).
[1] Equal contribution.

1566-1199/$ - see front matter © 2012 Elsevier B.V. All rights reserved.
http://dx.doi.org/10.1016/j.orgel.2012.03.037

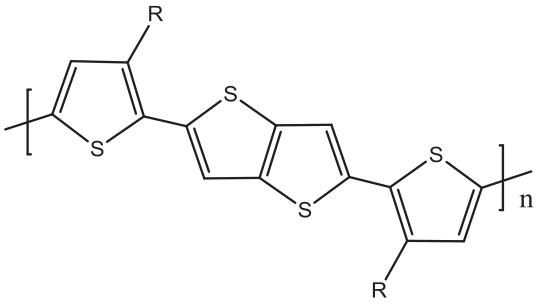

Fig. 1. Chemical structure of poly(2,5-bis(3-alkylthiophen-2-yl) thieno[3,2-b]thiophene). PBTTT derivates (–C10, R = $C_{10}H_{21}$; –C12, R = $C_{12}H_{25}$; –C14, R = $C_{14}H_{29}$).

(PBTTT in Fig. 1) has recently been synthesized for close packing of the macromolecule chains into large crystalline domains upon crystallization from a liquid crystal phase [6]. Due to the increased structure order and crystallinity, thin-film transistors made from PBTTT have been demonstrated to exhibit a hole mobility of 0.2–0.6 $cm^2 V^{-1} s^{-1}$ [7]. Pristine films of PBTTT, like P3HT, are composed of semi-crystalline lamellae separated by insulating alkyl chains, however films of PBTTT have a higher degree of crystallinity and order than films of P3HT because interdigitation of side-chains from adjacent lamellae occurs in PBTTT. Therefore, the use of such a high mobility semiconducting polymer in bulk-heterojunction solar cells has been investigated both in a single-layer bulk-heterojunction solar cell [8] and bilayer-bulk-heterojunction devices [9]. Nevertheless, the performance of those devices are unfavorable, because one may expect that BHJs containing PBTTT would suffer from poor exciton harvesting as the PBTTT could form large crystals that would expel the fullerene. However, Mayer et al. recently have demonstrated that fullerene derivatives intercalate between the polymer side chains in some polymer:fullerene blends, determining the optimal polymer:fullerene ratio to enhance the photovoltaic performance, since fullerenes must fill all available space between the polymer side chains prior to the formation of a pure electron-transporting fullerene phase in blends with intercalation [10].

In addition to the molecular-scale morphology, thermal stability is also an important property. Efficient bulk-heterojunction solar cells require the formation of an interpenetrating network of electron donor and acceptor materials with a large interfacial area. Heating induced

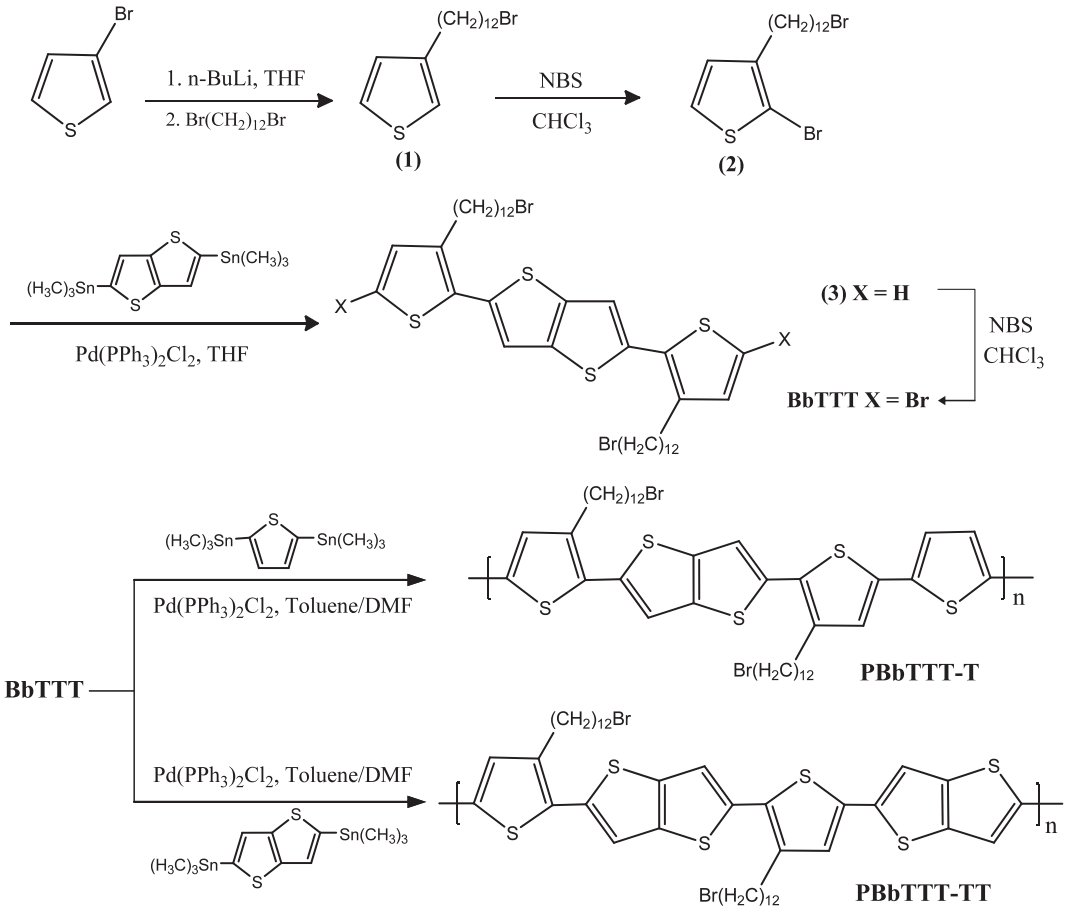

Scheme 1. Synthetic schemes for the 2,5-bis(3-bromododecylthiophen-2-yl) thieno[3,2-b]thiophene (**BbTTT**) and the corresponding copolymer **PBbTTT-T** and **PBbTTT-TT**.

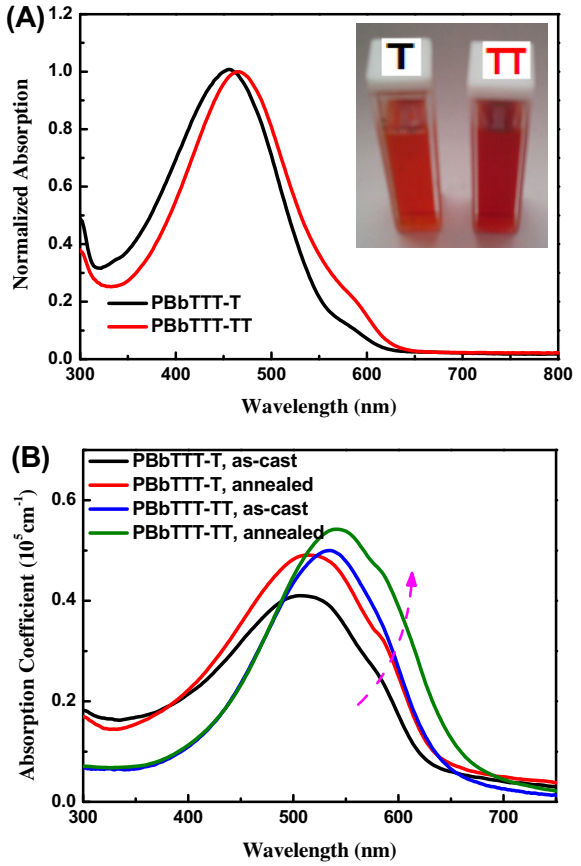

Fig. 2. (A) Normalized UV–vis absorption spectra of PBbTTT-T and PBbTTT-TT in solution, 10^{-5} mol/L in chloroform; and (B) solid absorption coefficients of the polymer films before and after annealing at 150 °C for 10 min. The insets in (A) shows the digital images of PBbTTT-T (T, left) and PBbTTT-TT (TT, right) in chloroform (10^{-3} mol/L).

by solar irradiation is detrimental to their performance because of the relatively low glass transition temperature (T_g) of the polymers and the possible macro-phase separation driven by the strong immiscibility between the active components. Although compatibilizer approaches [11] have been effective at enhancing the thermal stability, the synthesis of a compatibilizer often requires multiple post-polymerization steps and suffers from the low solubility of fullerenes. The ideal method is to lock-in the morphology by *in situ* compatibilization of donors and acceptors formed at the blend interface, achieving both solvent resistance and thermal stability [12]. Previously, we have demonstrated that the bromine-functionalized polythiophene upon photocrosslinking enables to suppress the morphology towards a state of macro-phase separation in the micrometer-size scale [13]. This situation inspires us to design a copolymer system with high crystalline (BTTT) and photocrosslinkable building blocks (Br-alkyl thiophene) for π–π intermolecular interactions that is, an alternating copolymer with liquid–crystalline nature and steadily donor–acceptor intercalated phase, to optimize processability, crystalline nanostructure and heat/solvent resistance.

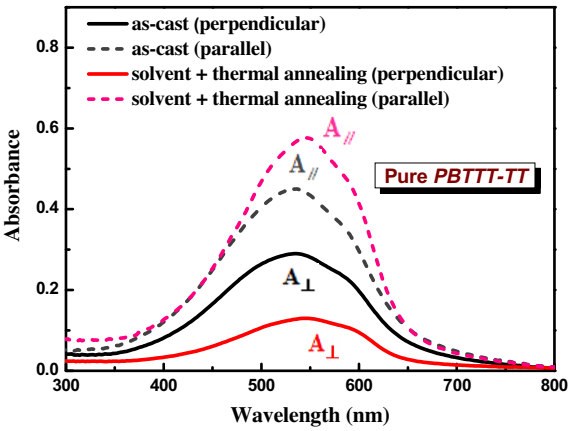

Fig. 3. UV–vis absorption spectra of the PBbTTT-TT film prepared in different conditions with linearly polarized incident light parallel or perpendicular to the long axis of the molecule direction, which is decided by the polarized absorption of corresponding films. The "as-cast film" is prepared in fast-grown, dried in vacuum. The "solvent + thermal" processing conditions is conducted firstly dried slowly in the covered petri dish and then thermally annealed at 150 °C for 10 min.

Table 1
Key polymer properties and optical property for PBbTTT derivates.

Polymer	M_n/PDI (kg/mol)	λ_{max}^{ab} [a] (nm)	λ_{max}^{ab} [b] (nm)	λ_{max}^{em} [c] (nm)	Extinction coefficient[d] (cm^{-1})	S [e]
PBbTTT-T	16.5/3.62	457	511/520	608/612	4.9×10^4	0.30
PBbTTT-TT	18.4/2.08	467	534/544	631/635	5.5×10^4	0.59
PBTTT-C12[f]	22.8/1.86	472	542/550	654/660	5.8×10^4	0.61

[a] Absorption spectra of polymer in solution (10^{-5} mol/L).
[b] Films UV–vis absorption spectra before and after annealing.
[c] Photoluminescence spectra of pristine films and annealed films, excited at 430 nm.
[d] Measured from annealed films absorption spectra at λ_{max} from annealed polymer film of Fig. 2.
[e] Order parameter S is calculated by $S = (A_{//} - A_{\perp})/(A_{//} + 2A_{\perp})$, measured from annealed films absorption spectra at λ_{max}.
[f] The value of polymer PBTTT-C12[poly(2,5-bis(3-dodecylthiophen-2-yl)thieno[3,2-b]thiophene)] is taking as the reference (Supplementary Fig. S5).

2. Results and discussion

On the basis of the idea to utilize this phenomenon, we designed novel polythiophene derivates with BTTT units and bromine-ended thiophene moieties, as shown in Scheme 1. The compound 3-bromododecylthiophene (**1**) was prepared according to a previously published process [14]. Then 2-bromo-3-(6-bromododecyl)thiophene (**2**) was synthesized by bromination of **1** with NBS, and 2,5-bis(3-bromododecylthiophen-2-yl)thieno[3,2-b]thiophene (**3**) was obtained by Stille coupling reaction between, then 5-dibromo-{2,5-bis(3-bromododecylthiophen-2-yl)thieno [3,2-b]thiophene}(BbTTT) was synthesized by bromination. The thiophene and thieno[3,2-b]thiophene units were incorporated regiospecifically at the 2,5 position into the

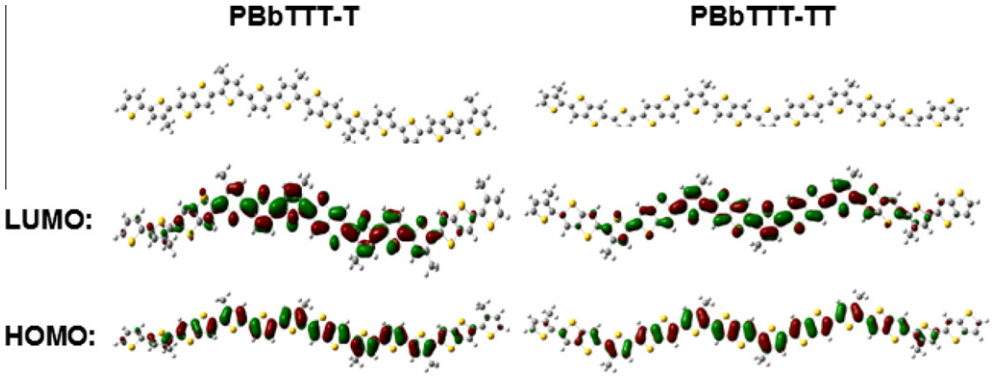

Fig. 4. HOMO and LUMO wave functions of the PBbTTT-T and PBbTTT-TT trimer model systems calculated at the ub3lyp/6-31g(d,p) level of theory.

Table 2
Electrochemical properties of the copolymers.

Polymers	HOMO (eV)	LUMO (eV)	HOMO (eV)[a]	E_g^{ec} (eV)[b]	E_g^{opc} (eV)[c]
PBbTTT-T	−4.91	−2.90	−4.69	2.01	1.96
PBbTTT-TT	−5.0	−3.10	−4.77	1.90	1.88

[a] Evaluated HOMO energy level of polymer trimer using DFT method at the ub3lyp/6–31g(d,p) level of theory.
[b] Calculated from $E_g = e(E_{onset/ox} - E_{onset/red})$.
[c] Calculated from the absorption band edge of the annealed copolymer films of Fig. 2, $E_g = 1240/\lambda_{edge}$.

polymer backbone by a 1:1 copolymerization with the BbTTT monomer, affording a series of copolymers poly[2, 5-bis(3-bromododecylthiophen-2-yl)thieno[3,2-b]thiophene-*alt*-2,5-thiophene] (PBbTTT-T) and poly[2, 5-bis (3-bromododecylthiophen-2-yl)thieno[3,2-b] thiophene-*alt*-2,5- thieno[3,2-b]thiophene] (PBbTTT-TT), to regulate the space between the side-chains (discussed lately). The structures of the copolymers were confirmed by ^{1}H-NMR, ^{13}C-NMR, and elemental analysis, compared with that of PBTTT-C12 to illustrate the structure difference. (Details in Supporting information) The presence of the bromine-alkyl functionality is confirmed by the appearance of new peak at about 3.43 ppm. After checking the structures of the polymers, the mesomorphic behaviors of copolymers are studied with polarizing optical microscopy (POM, Fig. S3) and differential scanning calorimetry (DSC, Fig. S4). When PBbTTT-T and PBbTTT-TT are cooled from its melt state, many anisotropic entities emerged from the background in both of the polymers. We found that both PBbTTT-T and PBbTTT-TT exhibits two discrete endotherm transitions on second heating, and two exothermic transitions on cooling. The first transition corresponds to the solid-mesophase transition, and the second corresponds to the mesophase-isotropic transition. In comparison with similar nematic extended hairy rod conjugated mainchain polymers, the relatively high enthalpies (over 10 J g^{-1}) of this transition suggests that the mesophase is semetic, which is further supported from XRD analysis [15].

The UV–vis absorption peaks of π-conjugated polymer films with crystallinity are usually red shifted relative to those measured in solution. This behavior is due to the enhanced intermolecular interactions between the polymer chains and the planarization effect of the π-conjugated polymer backbone, which render the polymer chains self-assemble into a well-ordered nanostructure in the solid state [16]. The extent of the red shift is related to the degree of order in the polymer; for example, the red shift can be up to 70 nm for some regioregular π-conjugated polymers, such as HT-P3HT, whereas there is only a small shift or no shift at all for others, such as HH-P3HT [17]. In Fig. 2, which shows the normalized UV–vis absorption spectra of PBbTTT-T and PBbTTT-TT in a chloroform solution and in the solid state casted from *o*-dichlorobenzene (DCB), the absorption peaks corresponding to the π–π∗ transitions of the polymer are present at 457 nm (511 nm in film) and 467 nm (534 nm in film), respectively. This large red shift suggests the presence of strong chain-to-chain interactions. It should be noted that the film absorption maxima of PBbTTT-TT, incorporating thieno[3,2-b]thiophene, red-shifts by ca. 20 nm, compared with PBbTTT-T in films. In addition, the effects of thermal annealing on the films are investigated using UV–vis absorption spectra (Fig. 2B). Importantly, after annealed at 150 °C for 10 min, the main absorption band red-shifts and the absorption is enhanced due to π–π stacking as well as the increasing intensity at the 590 nm shoulder peak, similar with absorption of reference polymer PBTTT-C12 (Fig. S5). The light sensitive Br-unit attached at the end of the dodecyl chain of PBbTTT derivates copolymers does not appear to disturb the π–π stacking of the backbone. Besides, the evolution of the polymer luminescence in the solid state as a function of the heat treatment is presented in Fig. S6A. The red-shift observed in the annealed films is likely attributed to efficient intermolecular interactions inside the aggregates, favored by the soft nature of liquid crystalline phase.

Moreover, the molecular packing can be enhanced through eliminating the disrupting of the planar conformation and ordering of the polymer, caused by rapid quenching of the solvent chains. If the growth rate of the active layer from solution to solid state is controlled, that is by "solvent annealing" [18], the intrinsic driving force for self-organization of PBbTTT derivates can lead to the high ordered structure. In order to study the molecular

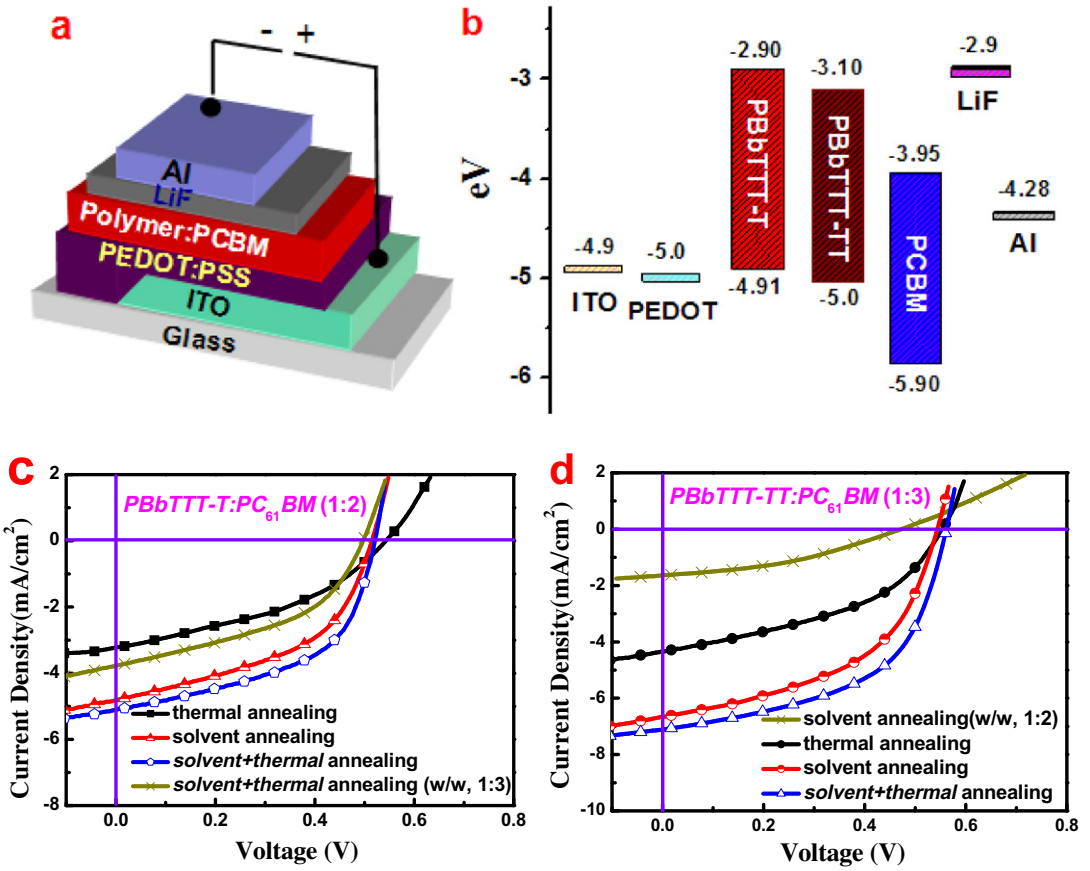

Fig. 5. (a) The device structure of polymer solar cells. (b) The energy level diagram of the corresponding components in the devices, in which the polymer energy levels are determined by cyclic voltammetry measurements. (c) *J–V* characteristics of devices (ITO/PEDOT:PSS/ PBbTTT-T:$PC_{61}BM$/LiF/Al) under different processing conditions, including varied blend ratios and annealing treatments. (d) *J–V* characteristics of devices (ITO/PEDOT:PSS/ PBbTTT-TT:$PC_{61}BM$/LiF/Al) under different processing conditions, including varied blend ratios and annealing treatments. Thermal annealing (the fast-grown films annealed at 150 °C for 10 min); "*solvent + thermal*" annealing conditions. (conducted firstly dried slowly in the covered petri dish and then thermally annealed)

orientation under varied treatments in thin solid film, the polarized absorption spectra (Fig. S7) are performed with the samples inserted between two polarizers with parallel and perpendicular directions from 50° to 330°. As shown in the Fig. 3, the absorption difference, calculated by order parameter *S*, indicates that the copolymer films treated with slow-grown and following LC phase annealing favors the best ordered molecular structure along the long axis direction [19]. Particularly, PBbTTT-TT shows a better packing behavior from the larger order parameter *S* (0.59) than polymer PBbTTT-T. These optical behaviors confirm that the co-monomer modification of PBbTTT-TT effectively promotes stronger intermolecular interaction in the solid state. Table 1 summarizes these important spectroscopic data.

Electrochemical cyclic voltammetry (CV, Fig. S8) was performed to determine the highest occupied molecular orbital (HOMO) and lowest unoccupied molecular orbital (LUMO) levels of PBbTTT-T and PBbTTT-TT. The polymer PBbTTT-TT shows a slightly lower-lying HOMO level at −5.0 eV, in agreement with the found high V_{OC} in the resultant devices; while PBbTTT-T exhibits a HOMO energy level of −4.91 eV. The lowest unoccupied molecular orbital (LUMO) levels of PBbTTT-T and PBbTTT-TT are determined to be −2.90 and −3.10 eV, respectively, that is, positioned more than 0.8 eV above that of electron acceptor PCBM (−3.95 eV, measured under the same conditions), which will ensure energetically favorable electron transfer. Furthermore, the features are in good agreement with the results of the optical bandgap of PBbTTT-TT deduced from its absorption edge in the solid state, which is determined to be 1.88 eV and narrower than that of PBbTTT-T (1.96 eV). This variation is also predicted by DFT calculations for the energy levels of each material. Pictorial representations of the HOMO and LUMO wave functions of the PBbTTT-T and PBbTTT-TT trimers are shown in Fig. 4, evaluated by DFT at the B3LYP/6-31g(d,p) level of theory. [20] With all the electrochemical data, the location of the HOMO and LUMO of the polymers are presented in Table 2.

To illustrate the difference of the PBbTTT derivates as the donor materials in the activelayer, BHJ solar cells are fabricated with the device structure, based on glass/ITO/PEDOT:PSS/polymer:PCBM/LiF/Al (Fig. 5a). The details on device fabrication process and characterization techniques

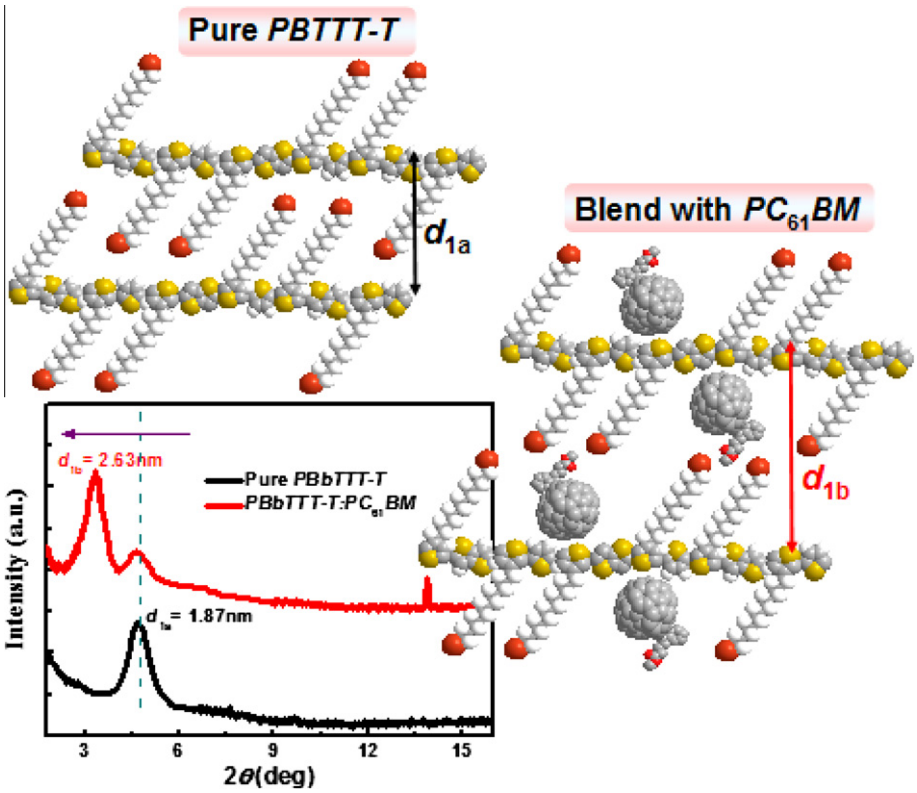

Fig. 6. Schematic of possible structures showing the effect of $PC_{61}BM$ intercalation on the crystal lattice of PBbTTT-T. (1, up) The tilt angle for the pure PBbTTT-T crystal and the amount of interdigitation of the side-chains is set to make the *d*-spacing (d_{1a}) agree with X-ray diffraction. (2, right) The $PC_{61}BM$ is placed within the intercalated PBbTTT-T:$PC_{61}BM$ (1:2) in order to agree with the expansion of *d*-spacings (d_{1b}) found in X-ray scattering (down).

Table 3
Summary of the processing conditions varied to optimize the device performance of PBbTTT-T:$PC_{61}BM$ system. (under A.M. 1.5, 100 mW/cm^2 irradiation)[a].

	Drying method	Thermal annealing	J_{sc}[b] (mA cm^{-2})	V_{oc}[c] (V)	FF[d]	η (%)
1:2	Slow	No	4.82	0.514	0.49	1.18
1:1	Slow	No	3.28	0.471	0.38	0.59
1:3	Slow	No	3.11	0.536	0.43	0.71
1:2[e]	Vacuum	No	2.68	0.541	0.38	0.55
1:2	Vacuum	150 °C, 10 min	3.22	0.544	0.40	0.69
1:2	Slow	150 °C, 10 min	5.11	0.520	0.52	1.38
1:2	Slow	150 °C, 30 min	4.72	0.509	0.48	1.15
1:3	Slow	150 °C, 10 min	3.78	0.496	0.45	0.84

[a]All values represent averages from six 0.04 cm^2 devices on a single chip.
[b]J_{sc} is the short-circuit current.
[c]V_{oc} is the open-circuit voltage.
[d]The fill factor (FF) is a graphic measure of the squareness of the *I–V* curve.
[e]Since the efficiencies of the 1:1 and 1:3 (wt.%) blends were considerably less than the efficiencies of the 1:2 blends, we used a 1:2 ratio for all subsequent optimization procedures. The highlighted entry shows the PBbTTT-T:$PC_{61}BM$ device with the highest efficiency.

are given in the characterizations section of supporting information [21]. Also, the map of HOMO and LUMO orbitals and the energy level of the materials are presented in Fig. 6b–d show the I–V curves for solar cells based on PBbTTT-T and PBbTTT-TT, respectively, under simulated AM 1.5 G radiation (100 mW/cm^2); optimized photovoltaic properties are summarized in Tables 3 and 4. As can be seen in the tables, the PSC device of PBbTTT-T with the active layer spincoated with fast dry method exhibits a poor performance with a PCE of only 0.55%. Conventional device optimization approaches, including donor/acceptor weight ratios, thermal annealing and solvent annealing have been applied to enhance the device performance; both short circuit current density (J_{sc}) and fill factor (FF) increase after annealing for all the three polymers, which can be explained by the enhanced ordered structure

Table 4
Summary of the processing conditions varied to optimize the device performance of PBbTTT-TT:PCBM system.

Blend ratio (w/w)	Drying method	Thermal annealing	J_{sc} (mA cm^{-2})	V_{oc} (V)	FF	η (%)
PBbTTT-TT:$PC_{61}BM$[a]						
1:2	Slow	No	1.64	0.471	0.38	0.30
1:3	Slow	No	6.67	0.543	0.50	1.80
1:4	Slow	No	6.10	0.545	0.49	1.62
1:3[b]	Vacuum	No	4.34	0.553	0.44	1.04
1:3	Vacuum	150 °C, 10 min	5.51	0.568	0.51	1.58
1:3	Slow	150 °C, 10 min	7.11	0.561	0.54	2.14
1:3	Slow	150 °C, 30 min	6.08	0.549	0.48	1.60
1:4	Slow	150 °C, 10 min	4.32	0.540	0.45	1.06
PBbTTT-TT:$PC_{71}BM$[c]						
1:3	Slow	No	5.39	0.564	0.43	1.30
1:3.5	Slow	No	7.84	0.577	0.57	2.57
1:4	Slow	No	7.09	0.548	0.51	1.98
1:3.5	Slow	150 °C, 10 min	6.56	0.554	0.44	1.60
1:4(PBTTT)[d]	Slow	No	8.32	0.559	0.55	2.58

[a]The acceptor materials used in this series is $PC_{61}BM$ ([6,6]-phenyl-C61-butyric acid methyl ester).
[b]Since the efficiencies of the 1:2 and 1:4 (wt.%) blends were considerably less than the efficiencies of the 1:3 blends, we used a 1:3 ratio for all subsequent optimization procedures of PBbTTT-TT:$PC_{61}BM$ blends.
[c]The acceptor materials used in this series is $PC_{71}BM$ ([6,6]-phenyl-C71-butyric acid methyl ester).
[d]The highest efficiency values and conditions of PBTTT-C12:$PC_{71}BM$ are showed as the reference. The highlighted entry shows the PBbTTT-TT:$PC_{61}BM$ and PBbTTT-TT:$PC_{71}BM$ devices with the highest efficiency, respectively.

formation in the thin films. However, all results of PBbTTT-T are inferior to that of PBbTTT-TT in the similar processing conditions. Particularly, the optimal weight ratios of PBbTTT-T:$PC_{61}BM$ (1:2) blend is below that of PBbTTT-TT:$PC_{61}BM$ (1:3).

Since the performance of polymer:fullerene bulk heterojunction solar cells is heavily influenced by the nanostructure formed by the two semiconductors because the size of the phases, the nature of the interface, molecular packing affect exciton dissociation, recombination, and charge transport. To gain deep insight into the effect of optimum blend ratios on performance, it is important to understand how intercalation between polymers and fullerene affects device performance. X-ray diffraction is used to determine whether the intercalation occurs in polymer:fullerene blends, and the results show that intercalation causes an increase in the lamellar spacing of the polymer as shown in Figs. 6 and 7 with space-filling schematic made from ChemDraw3D [22]. Pristine films of PBbTTT-T have a high degree of order that stems from interdigitation of the side-chains. X-ray diffraction of $PC_{61}BM$ blended with PBbTTT-T having dodecyl side-chains shows a suppression of the diffraction, but also appears a shift to larger *d*-spacing. It suggests that the fullerenes affect part of the interaction between the polymer chains. And the fullerenes can only intercalate between the side chains of PBbTTT-T with larger space of dimer model and that a bimolecular crystal forms as shown in the inset to Fig. 6. The X-ray pattern in this figure shows that upon intercalation there is a 7.6 Å shift, from 18.7 to 26.3 Å, in the d-spacing for a 1:2 blend of PBbTTT-T:$PC_{61}BM$. Not similar with the PBTTT, X-ray diffraction of $PC_{61}BM$ blended with PBbTTT-T shows a reduction of the original diffraction and a new peak, rather than a shift completely. It is due to that the bimolecular crystal only forms with the longer side-chains, because the fullerene does not completely fill the space between the side-chains and leaves room for side-chain interdigitation. It is similar with the previously reported conditions of poly(terthiophene) (PTT) [23]. However, in contrast to the polymers PBbTTT-T, the highly crystalline PBbTTT-TT with more symmetric structure has sufficient room for intercalation as shown in the Fig. 7. The annealing took place at the mesophase temperature (150 °C) of PBbTTT-TT have been conducted to increase the molecular order. (Fig. S9) X-ray scattering for a pure PBbTTT-TT film is almost consistent with the literature of PBTTT and displays several diffraction orders [24]. With the addition of more fullerenes to the ratio of 1:3, the peak corresponding to the intercalated lattice shifts and the peak associated with the 19.6 Å (4.52°) is completely suppressed. The existence of new sets of peaks in the 1:3 films (with an expanded *d*-spacing of 27.6 Å) suggests that the fullerenes are not largely breaking the uniformity throughout the film.

For the 1:2 PBbTTT-TT:$PC_{61}BM$ blend, the low current and the resulting low efficiency can be attributed to the inability of electrons to be extracted from the device due to the absence of an electron-conducting phase (pure fullerene). When more intercalation occurs, a higher level of fullerene-loading is necessary to create the phase separation needed for efficient BHJ solar cells. However, additional loading of fullerene to 80 wt.% has little positive effect, and aggregation of the redundant and free $PC_{61}BM$ after thermal annealing leads to severe phase separation of PCBM crystals (Fig. S10). Besides the photovoltaic performance, the optimize blending is proved from the photoluminescence spectra (Fig. S6B) because PL is often used as an indicator of how well excitons can diffuse to a donor–acceptor interface, where they can be split into free charges, since PL occurs when the excitons recombine emissively prior to splitting. The PL of pure PBbTTT-TT is virtually 100% quenched when increasing the $PC_{61}BM$ containing to 75%, near a 1:3 ratio so that there are approximately equal volumes of the intercalated phase, which

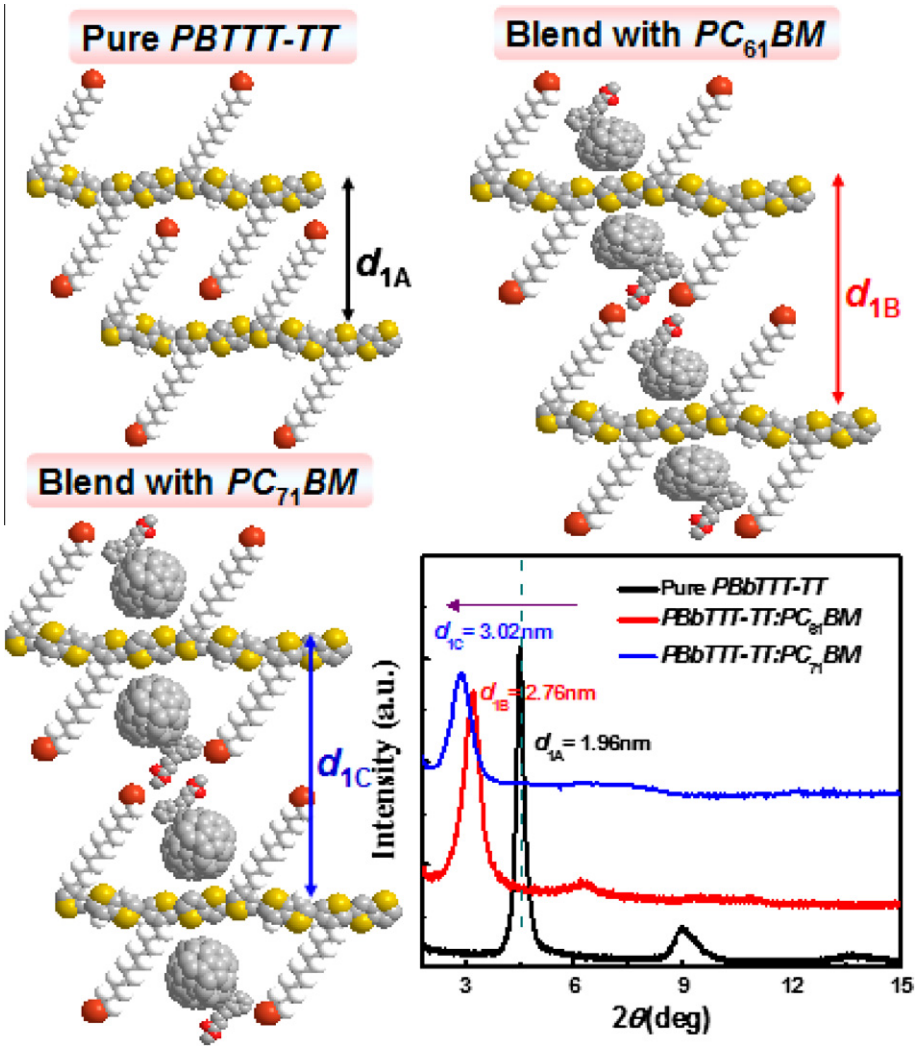

Fig. 7. Schematic of possible structures showing the effect of $PC_{61}BM$ and $PC_{71}BM$ intercalation on the crystal lattice of PBbTTT-TT. (1, upper left) The tilt angle for the pure PBbTTT-T crystal and the amount of interdigitation of the side-chains is set to make the *d*-spacing (d_{1A}) agree with X-ray diffraction (lower right). (2, upper right) The $PC_{61}BM$ is placed within the intercalated PBbTTT-TT:$PC_{61}BM$ (1:3) in order to agree with the increasing *d*-spacings (d_{1B}) found in X-ray scattering (lower right). (3, lower left) The $PC_{71}BM$ is placed within the intercalated PBbTTT-TT:$PC_{71}BM$ (1:3.5) in order to agree with the more increasing *d*-spacings (d_{1C}) found in X-ray scattering (lower right).

Table 5
Fullerene intercalation in a variety of polymer:PCBM systems. The molecular weights are 911 and 1031 g mol^{-1} for $PC_{61}BM$ and $PC_{71}BM$, respectively.

Polymers	M_w of monomer g mol^{-1}	Monomers/fullerene[a]	Ideal% $PC_{61}BM$ (Ideal% $PC_{71}BM$)	Experimental optimum
PBbTTT-T	876	2 (n = 0.5)	67.1(68.6)	66.7(–)
PBbTTT-TT	935	1 (n = 1)	74.7(76.2)	75(77)
PBTTT-C12	638	1 (n = 1)	79.4(80.9)	80(80)

[a] The values of monomers to fullerenes, n are determined from scale drawings of the chemical structures similar to Figs. 6 and 7.

has about one fullerene per monomer, and the pure fullerene phase. McGehee et al. [25] have shown that BHJ solar cells work best when they consist of a bicontinuous network with approximately equal volumes of electron-transporting (pure fullerene) and hole-transporting (intercalated phase or pure polymer) domains in order to have equal paths for electrons and holes and minimize the density of dead-ends. The fullerene weight percentage needed to match the volumes of the electron-transporting and the hole-transporting regions, assuming that the polymer and intercalated phase have the same density, is given by the equation [25a],

$$x = \frac{100n\zeta + 50}{1 + n\zeta}$$

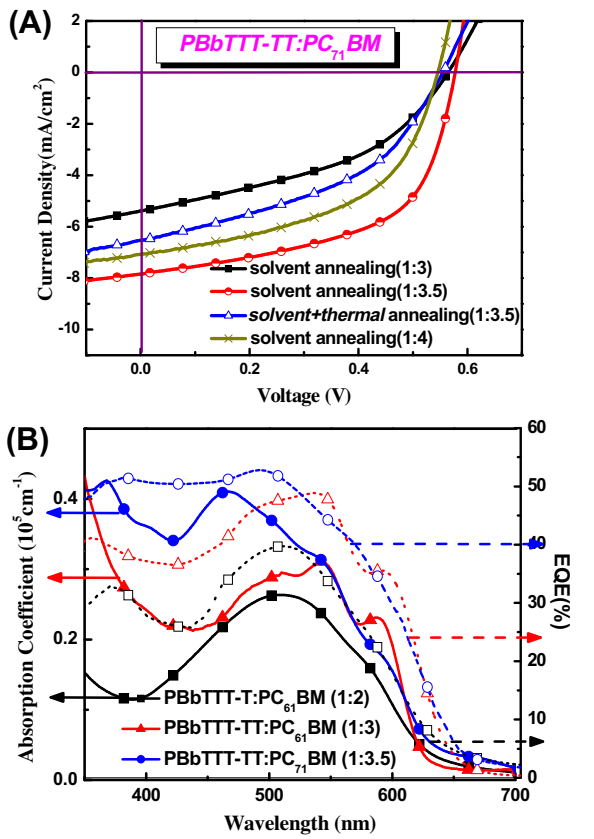

Fig. 8. (A) *J–V* characteristics of device (ITO/PEDOT:PSS/PBbTTT-TT:$PC_{71}BM$/LiF/Al) under different processing conditions, including varied blend ratios and annealing treatments. (B) IPCE and absorption spectra for the highest efficiency BHJ devices derived from PBbTTT-T:$PC_{61}BM$ and PBbTTT-TT:$PC_{61}BM$ and PBbTTT-TT:$PC_{71}BM$.

where ζ is the molecular weight ratio of the fullerene to the monomer and n is the number of fullerenes per monomer in the intercalated phase. The value of n was determined by the scale drawings of the chemical structures similar to Figs. 6 and 7. If fullerenes can only intercalate between the longer bimolecular crystal side-chains, $n = 0.5$. Table 5 compares the value of x for several polymer:fullerene BHJs to the experimentally optimized blending ratios found in this study and shows that this simple formula consistently predicts the optimal blending ratio.

On the other hand, although there is enough space between the side-chains to accommodate the fullerenes, blending $PC_{71}BM$ with PBbTTT-TT further increase the lamellar spacing. And the increasing spacing (d-spacing of 30.2 Å) is most likely attributed to the larger fullerene cage, which enlarges the lamellar stack between the polymer side chains. Meanwhile, the increasing molecular weights of $PC_{71}BM$ lead to the optimal blending ratio of the activelayer to 1:3.5. The enhanced absorption of $PC_{71}BM$ (in the wavelength region of 380–500 nm) [26] explains the higher current (7.8 mA cm^{-2}) in the PBbTTT-TT:$PC_{71}BM$ versus the PBbTTT-TT:$PC_{61}BM$ blends, leading to the PCE up to 2.57% (Fig. 8A), close values with PBTTT-C12:$PC_{71}BM$. This performance improvement is confirmed from integrated incident photon–to–current conversion efficiency (IPCE) spectra, which is consistent with the absorption spectra of the blends (Shown in Fig. 8B).

The nanoscale morphology of the active layer can be smartly controlled by the annealing treatments. As the fullerene molecules are trapped within the polymer crystal, the thermally induced self-ordering of the chain also poses a positive effect on the electron transport. Encouragingly, by 150 °C annealed treatment for 10 min, the PCE of PBbTTT-TT:$PC_{61}BM$ (1:3) is improved to 2.14% as a result of the simultaneously increased *J*sc and FF values. (Fig. 5d) However, for the $PC_{71}BM$ blends, the thermal treatments disrupt the device performance. The reason for this may be attributed to that the larger volume $PC_{71}BM$ can hardly be located within the interpenetrating network after exposure to heat and annealing the blends with $PC_{71}BM$ domains causes the free $PC_{71}BM$ aggregating, creating discontinuous pathways. As shown in the SEM topographs and optical micrographs of Fig. 9, as well as the root mean square (rms) roughnesses given in Table 6, only the active-layer of PBbTTT-TT:$PC_{71}BM$ annealed at 150 °C exhibits a very rough surface with plenty of large particles. The micro-particle of fullerene aggregates causes the phase separation and reduction in the n-type mobility, leading to the unbalanced hole and electron transport estimated by space charge limited current (SCLC) mode [27]. The less-mobile electrons left behind in the bulk will form a space–charge region thus affecting the *J–V* characteristics of the blend. For devices comprising $PC_{71}BM$ films annealed at 150 °C, device series resistance, R_{SA}, increases from 1.2 to 10.9 Ω cm^{-2}, underlining the effect of discontinuous pathways.

To play the advantage of photocrosslinking and facilitate comparison, the pre-optimum morphology has been employed; and the procedures of device preparation are conducted under various optimization polymer:PCBM blends in the former discussion. Photocrosslinking is carried out under inert argon atmosphere using UV light ($\lambda = 254$ nm) from a low power hand-held lamp with exposure time about 30 min. The photocrosslinking behavior of Br content is clearly confirmed by the insolubility of the films in DCB, which is speculated via a radical mechanism initiated by the photochemical cleavage of the C–Br bonds under deep UV irradiation [28]. Fig. 10A presents a comparison of active-layer made from pristine PBbTTT-T:$PC_{61}BM$ and PBbTTT-TT:$PC_{61}BM$; crosslinked PBbTTT-T:$PC_{61}BM$ and PBbTTT-TT:PCBM ($PC_{61}BM$ and $PC_{71}BM$) films on ITO substrate before and after washing with DCB. The pristine films are completely washed out, while the films exposed to UV irradiation for 30 min remain intact. These results clearly demonstrate that our photo-crosslinking approach is an efficient method of achieving solvent-resistant activelayer and stable charge transport under an organic solvent. And it shows that the crosslinkable polymer can operate under a harsh environment such as organic solvent wastes. In addition to solvent resistance, enhancing thermal stability in organic electronics, particularly in BHJ OPVs, is of great importance. To investigate the effect of photocrosslinkable PBbTTT copolymers on the thermal stability of the solar cells, the performance of PBTTT-C12, PBbTTT-T and PBbTTT-TT with PCBM blends, including various acceptors ($PC_{61}BM$ and

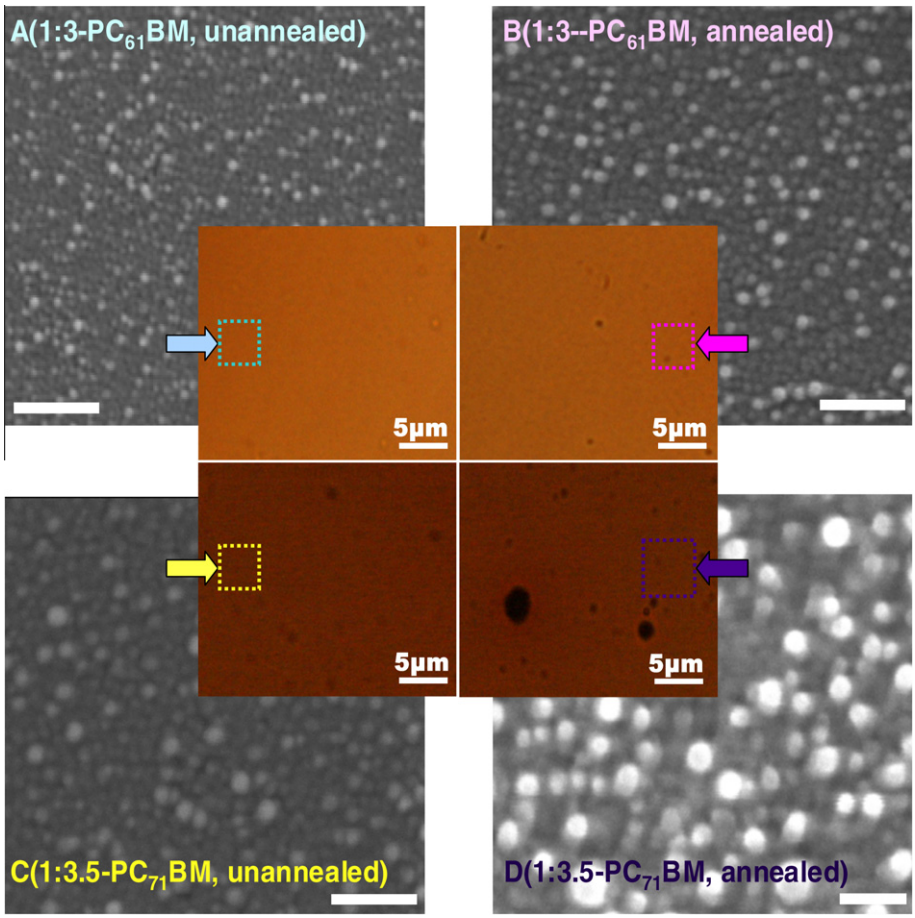

Fig. 9. SEM topographs (the bar: 500 nm) and optical micrographs of PBbTTT-TT:$PC_{61}BM$ (1:3, w/w) and PBbTTT-TT:$PC_{71}BM$ (1:3.5, w/w) transistors before and after annealing at 150 °C for 10 min. 1:3 Blending of PBbTTT-TT:$PC_{61}BM$ is almost unaffected by the annealing process, while the aggregated fullerene clusters are formed in the annealed sample of PBbTTT-TT:$PC_{71}BM$. This lead to a reduction in n-type mobility in the annealed samples as shown in Table 5.

Table 6
X-ray diffraction results and space-charge-limited conductivity (SCLC) measured hole mobilities for PBbTTT-TT:$PC_{61}BM$ (1:3, w/w) and PBbTTT-TT:$PC_{71}BM$ (1:3.5, w/w) activelayer films.

Active layer	SCLC measurement		XRD measurement		Roughness σ[a] (rms) (nm)	R_{SA}[b] (Ω cm^{-2})
	Hole mobilities ($cm^2 V^{-1} s^{-1}$)	Electron mobilities ($cm^2 V^{-1} s^{-1}$)	2θ (°)	d-Spacing (Å)		
PBbTTT-TT:$PC_{61}BM$ solvent[a]	5.61×10^{-4}	1.02×10^{-4}	3.24	27.1	5.2	8.2
PBbTTT-TT:$PC_{61}BM$ solvent and thermal[b]	1.02×10^{-3}	6.71×10^{-4}	3.20	27.6	6.9	3.0
PBbTTT-TT:$PC_{71}BM$ solvent	7.23×10^{-4}	3.83×10^{-4}	2.92	30.2	6.3	1.2
PBbTTT-TT:$PC_{71}BM$ solvent and thermal	8.31×10^{-4}	2.46×10^{-5}	2.96	29.7	15.8	10.9

[a] The data are derived from AFM surface topology images from Supplementary Fig. S11.
[b] The series resistance of the corresponding devices.

$PC_{71}BM$), are measured as a function of annealing time at 150 °C (Fig. 10B). Initially, PBTTT-C12:$PC_{71}BM$ and PBbTTT-TT:$PC_{71}BM$ blended devices show almost identical PCE performance. However, they show a dramatic contrast in thermal stability after annealing at an elevated temperature of 150 °C for 5 h. The performance of the two PBbTTT-TT ($PC_{61}BM$ and $PC_{71}BM$) devices treated by UV irradiation for 30 min showed very stable device performance even after 40 h of annealing at 150 °C, especially for PBbTTT-TT:$PC_{71}BM$ (94% initial device efficiency). This perfor-

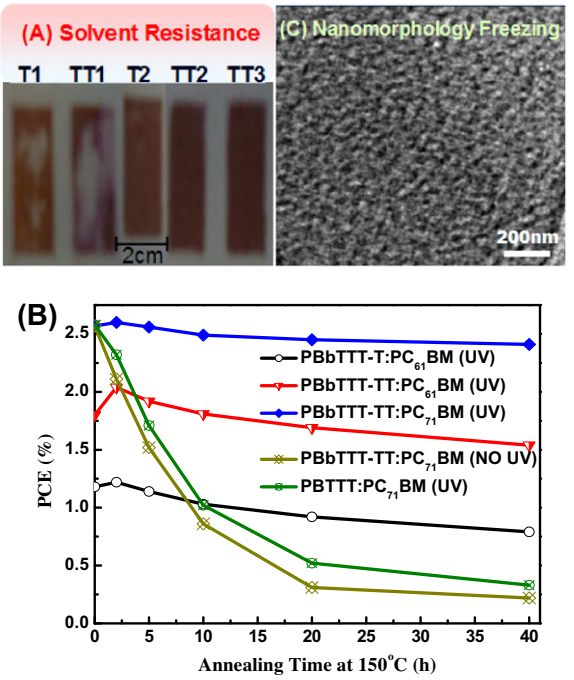

Fig. 10. (A) Comparison solvent-resistant performance of pristine PBbTTT-T:$PC_{61}BM$ (T1) and PBbTTT-TT:$PC_{61}BM$ (TT1); photo-crosslinked PBbTTT-T:$PC_{61}BM$ (T2), PBbTTT-TT:$PC_{61}BM$ (TT2) and PBbTTT-TT:$PC_{71}BM$ (TT3) films. (B) Efficiencies of devices based on polymers of PBTTT, PBbTTT-T and PBbTTT-TT annealed at 150 °C for different times. Five different devices were prepared under identical condition except the ratio of polymer to PCBM:PBbTTT-T:$PC_{61}BM$ (1:2, w/w), PBbTTT-TT:$PC_{61}BM$ (1:3, w/w), PBbTTT-TT:$PC_{71}BM$ (1:3.5, w/w) and PBTTT-C12:$PC_{71}BM$ (1:4, w/w); and with (**UV**) or without (**NO UV**) being exposed to UV 30 min. (C) TEM image of PBbTTT-TT:$PC_{71}BM$ (1:3.5, w/w) activelayer film under 150 °C annealing for 10 h.

mance, to the best of our knowledge, represents one of the most thermally stable polymer BHJ devices (90% initial device efficiency of bromine-functionalized polythiophene) [12c]. In contrast, the devices performance based on PBTTT-C12:$PC_{71}BM$ decrease rapidly to less than a third of its initial efficiency value after 10 h at 150 °C. Similarly, a control sample of PBbTTT-TT:$PC_{71}BM$ without any UV treatment shows a rapid decrease in device performance after long heating. This result clearly shows that the photocrosslinking concept holds promise for thermally stable high performance devices. The effects of UV crosslinking on freezing this optimum intercalated-phase morphology of PBbTTT-TT:$PC_{71}BM$ blend (Fig. 10C) as well as the crystalline structures is responsible for the long term performance, which avoid the fullerene aggregates in the non-crosslinked devices. It is notable that the thermal stability of $PC_{71}BM$ blend outperforms the $PC_{61}BM$ devices. The clear advantage of $PC_{71}BM$ over $PC_{61}BM$ blend may be attributed to the less free space between the side-chains of PBbTTT-TT and $PC_{71}BM$ after the intercalation, which can fix the fullerene in the crosslinked network and prevent PCBM from slipping away. And this factor of free space to the stability is further proved by the worse stability of the devices based on PBbTTT-T:$PC_{61}BM$ (67% initial device efficiency) with more free room after the intercalation between fullerenes and bimolecular crystal of polymer PBbTTT-T.

The effects of UV crosslinking on the morphology can be gleaned by examination of the morphology of the active layer via optical microscopy. Fig. 11 shows the optical microscopy images of PBbTTT-TT:$PC_{61}BM$ (1:3) and PBbTTT-TT:$PC_{71}BM$ (1:3.5) with or without UV crosslinking after 24 h thermal annealing. These images demonstrate that thermal annealing at 150 °C induces the formation of many needle-like PCBM crystals that are over 5 μm in length in the activelayer films without crosslinked by UV treatment as seen in Fig. 11B and D indicating that there are severe macrophase separation driven by the crystallization of the highly regioregular PBbTTT-TT polymer and PCBM molecule. In contrast, in Fig. 11C, the optical micrograph of the PBbTTT-TT:$PC_{71}BM$ blend crosslinked by UV treatment shows a homogeneous film free of dark PCBM crystals. These optical micrographs confirm that the photocrosslinking serves to freeze this optimized nanomorphology and suppresses phase segregation, thus producing stable performance in solar cell devices. We also note that there are visible phase-separation in the crosslinked PBbTTT-TT:$PC_{61}BM$ film (Fig. 11A), which is consistent with the relatively poor stability (85% initial device efficiency after 40 h). Therefore, these discoveries suggest why large-scale phase separation occurs in some polymer:fullerene blend ratios while thermally stable mixing on the molecular scale occurs for others. And the system provides a method of intentionally designing bimolecular crystals and tuning their size to create suitable material for BHJ devices with high stability.

3. Conclusions

In this study, new liquid crystalline PBbTTT derivates copolymers are successfully synthesized to enhance the stability of organic electronic devices using photocrosslinkable bromine-functionalized units. The light sensitive unit attached at the end of the dodecyl chain of PBbTTT-T and PBbTTT-TT does not disturb the π–π stacking of the PBbTTT backbone from the oriented molecular packing behavior. After compared the properties of polymer:fullerene blends with and without intercalation using X-ray diffraction, current–voltage measurements, photoluminescence and morphology characteristics, the different space-filling schematic have been obtained and optimum donor/acceptor blending ratios for PBbTTT-T:$PC_{61}BM$, PBbTTT-TT:$PC_{61}BM$ and PBbTTT-TT:$PC_{71}BM$ are 1:2, 1:3 and 1:3.5, respectively. When more intercalation occurs, a higher level of fullerene-loading is necessary to create the phase separation needed for efficient BHJ solar cells. The best cells with intercalation are 2.57% efficient, while the best cells with half-intercalation are 1.38% efficient. When the intercalation occurs, a clear advantage for photocrosslinking strategy is that crosslinking can be used in order to freeze this optimum morphology of donor–acceptor bicontinuous network and preserve long term performance. A comparison of the blend morphology indicates that the equivalent fullerene size and side-chain spacing of polymer have been determined to create the best steadily intercalated nanostructure. As a result,

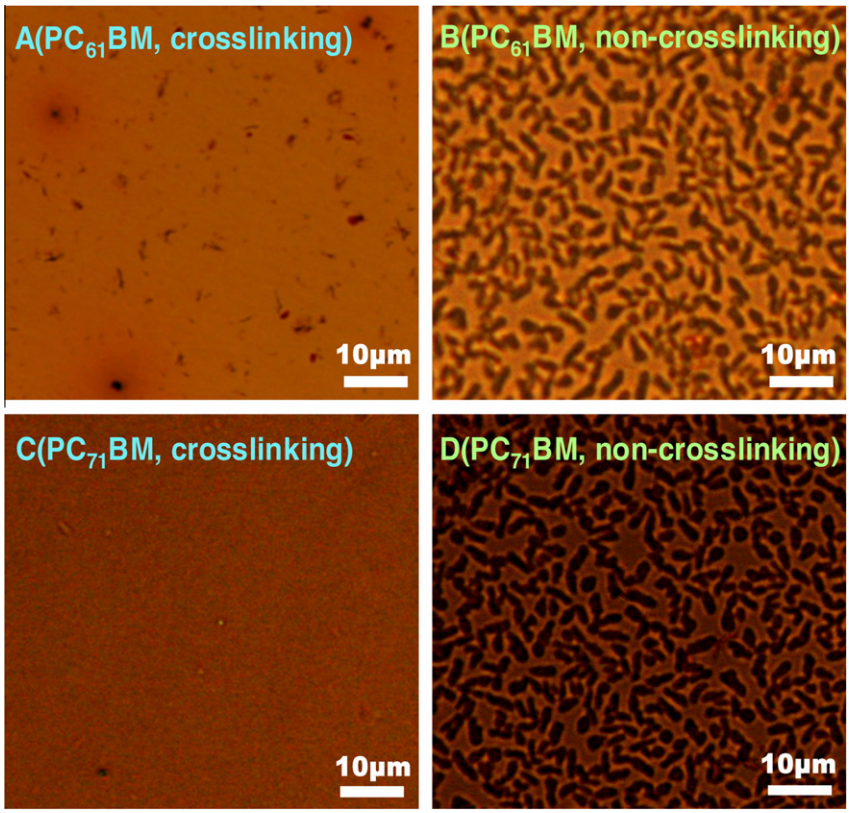

Fig. 11. Optical micrographs of PBbTTT-TT:$PC_{61}BM$ (1:3, w/w) and PBbTTT-TT:$PC_{71}BM$ (1:3.5, w/w) transistors annealing at 150 °C for 24 h with or without exposure to UV for 30 min. Dark areas are PCBM-rich regions. $PC_{71}BM$ blending of PBbTTT-TT is unaffected by the annealing process.

BHJ solar cells based on PBbTTT-TT:$PC_{71}BM$ show remarkably enhanced thermal stability, 94% initial device efficiency after 40 h annealing, when compared with PBbTTT-T:$PC_{61}BM$ and PBbTTT-TT:$PC_{61}BM$, let alone the conventional devices utilizing a PBTTT-C12:$PC_{71}BM$ blend.

Acknowledgments

This work was supported by the National Natural Science Foundation of China (51073076 and 51003045) and Graduate Innovation Fund Projects of Jiangxi Province (YC10A023).

Appendix A. Supplementary data

Supplementary data associated with this article can be found, in the online version, at http://dx.doi.org/10.1016/j.orgel.2012.03.037.

References

[1] (a) Y. Liang, Z. Xu, J. Xia, S.-T. Tsai, Y. Wu, G. Li, C. Ray, L. Yu, Adv. Mater. 22 (2010) E135–E138;
(b) A.W. Hains, Z. Liang, M.A. Woodhouse, B.A. Gregg, Chem. Rev. 110 (2010) 6689–6735.
[2] F.C. Krebs, Sol. Energy Mater. Sol. Cells 93 (2009) 394–412.
[3] (a) R.F. Service, Science 332 (2011) 293;
(b) Z. He, C. Zhong, X. Huang, W.-Y. Wong, H. Wu, L. Chen, S. Su, Y. Cao, Adv. Mater. 23 (2011) 4636–4643.
[4] (a) J.M. Nunzi, Compt. Rend. Physique 3 (2002) 523–542;
(b) P.E. Shaw, A. Ruseckas, I.D.W. Samuel, Adv. Mater. 20 (2008) 3516–3520;
(c) Y. Zhang, H.-L. Yip, O. Acton, S.K. Hau, F. Huang, A.K.-Y. Jen, Chem. Mater. 21 (2009) 2598–2600.
[5] (a) C.J. Brabec, M. Heeney, I. McCulloch, J. Nelson, Chem. Soc. Rev. 40 (2011) 1185–1199;
(b) R. Po, M. Maggini, N. Camaioni, J. Phys. Chem. C 114 (2010) 695–706;
(c) H. Yan, Z.H. Chen, Y. Zheng, C. Newman, J.R. Quinn, F. Dotz, M. Kastler, A. Facchetti, Nature 457 (2009) 679–686.
[6] I. McCulloch, M. Heeney, C. Bailey, K. Genevicius, I. MacDonald, M. Shkunov, D. Sparrowe, S. Tierney, R. Wagner, W. Zhang, M.L. Chabinyc, R.J. Kline, M.D. McGehee, M.F. Toney, Nat. Mater. 5 (2006) 328–333.
[7] (a) L.A. Lucas, D.M. DeLongchamp, B.M. Vogel, E.K. Lin, I. McCulloch, M. Heeney, G.E. Jabbour, Appl. Phys. Lett. 90 (2007) 012112;
(b) R.J. Kline, D.M. DeLongchamp, D.A. Fischer, E.K. Lin, M. Heeney, I. McCulloch, M.F. Toney, Appl. Phys. Lett. 90 (2007) 062117.
[8] I.-W. Hwang, J.Y. Kim, S. Cho, J. Yuen, N. Coates, K. Lee, M. Heeney, I. McCulloch, D. Moses, A.J. Heeger, J. Phys. Chem. C 112 (2008) 7853–7857.
[9] Q. Sun, K. Park, L. Dai, J. Phys. Chem. C 113 (2009) 7892–7897.
[10] (a) N.C. Cates, R. Gysel, Z. Beiley, C.E. Miller, M.F. Toney, M. Heeney, I. McCulloch, M.D. McGehee, Nano Lett. 9 (2009) 4153–4157;
(b) J.E. Parmer, A.C. Mayer, B.E. Hardin, S.R. Scully, M.D. McGehee, M. Heeney, I. McCulloch, Appl. Phys. Lett. 92 (2008) 113309.
[11] (a) R. Png, P. Chia, J. Tang, B. Liu, S. Sivaramakrishnan, M. Zhou, S. Khong, H.S.O. Chan, J.H. Burroughes, L. Chua, R.H. Friend, P.K.H. Ho, Nat. Mater. 9 (2010) 152–158;
(b) N. Cho, H.-L. Yip, J.A. Davies, P.D. Kazarinoff, D.F. Zeigler, M.M.

Durban, Y. Segawa, K.M. O'Malley, C.K. Luscombe, A.K.-Y. Jen, Adv. Energy Mater. 1 (2011) 1148–1153;
(c) S. Miyanishi, Y. Zhang, K. Tajima, K. Hashimoto, Chem. Commun. 46 (2010) 6723–6725.
[12] (a) S. Miyanishi, K. Tajima, K. Hashimoto, Macromolecules 42 (2009) 1610–1618;
(b) Y.J. Cheng, C.H. Hsieh, P.J. Li, C.S. Hsu, Adv. Funct. Mater. 21 (2011) 1723–1732;
(c) B.J. Kim, Y. Miyamoto, B. Ma, J.M.J. Fréchet, Adv. Funct. Mater. 19 (2009) 2273–2281;
(d) H.J. Kim, A.-R. Han, C.-H. Cho, H. Kang, H.-H. Cho, M.Y. Lee, J.M.J. Fréchet, J.H. Oh, B.J. Kim, Chem. Mater. 24 (2011) 215–221.
[13] (a) X. Li, L. Chen, Y. Chen, F. Li, K. Yao, Org. Electron. 13 (2012) 104–113;
(b) K. Yao, L. Chen, F. Li, P. Wang, Y. Chen, J. Phys. Chem. C 116 (2011) 714–721.
[14] (a) L. Zhai, R.L. Pilston, K.L. Zaiger, K.K. Stokes, R.D. McCullough, Macromolecules 36 (2003) 61–64;
(b) K. Yao, L. Chen, Y. Chen, F. Li, P. Wang, J. Mater. Chem. 21 (2011) 13780–13784.
[15] (a) M. Heeney, C. Bailey, M. Giles, M. Shkunov, D. Sparrowe, S. Tierney, W. Zhang, I. McCulloch, Macromolecules 37 (2004) 5250–5256;
(b) J.W.Y. Lam, Y.P. Dong, K.K.L. Cheuk, Z.L. Xie, H.S. Kwok, Z.S. Mo, B.Z. Tang, Macromolecules 35 (2002) 1229–1240.
[16] (a) B.S. Ong, Y. Wu, P. Liu, S. Gardner, J. Am. Chem. Soc. 126 (2004) 3378–3379;
(b) H. Kokudo, T. Sato, T. Yamamoto, Macromolecules 39 (2006) 3959–3963.
[17] (a) T. Kawase, T. Shimoda, C. Newsome, H. Sirringhaus, R.H. Friend, Thin Solid Films 438–439 (2003) 279–287;
(b) W.C. Tsoi, S.J. Spencer, L. Yang, A.M. Ballantyne, P.G. Nicholson, A. Turnbull, A.G. Shard, C.E. Murphy, D.D.C. Bradley, J. Nelson, J.-S. Kim, Macromolecules 44 (2011) 2944–2952.
[18] G. Li, V. Shrotriya, J.S. Huang, Y. Yao, T. Moriarty, K. Emery, Y. Yang, Nat. Mater. 4 (2005) 864–868.
[19] (a) T. Nishizawa, L. Hadykesuma, K. Tajima, K. Hashimoto, J. Am. Chem. Soc. 131 (2009) 2464–2465;
(b) K. Ichimura, Chem. Rev. 100 (2000) 1847–1873.
[20] (a) M.C. Scharber, D. Wuhlbacher, M. Koppe, P. Denk, C. Waldauf, A.J. Heeger, C.L. Brabec, Adv. Mater. 18 (2006) 789–794;
(b) S. Ko, R. Mondal, C. Risko, J.K. Lee, S. Hong, M.D. McGehee, J.L. Bredas, Z. Bao, Macromolecules 43 (2010) 6685–6698.
[21] K. Yao, Y.W. Chen, L. Chen, F. Li, X.E. Li, X.Y. Ren, H.M. Wang, T.X. Liu, Macromolecules 44 (2011) 2698–2706.
[22] (a) R.J. Kline, D.M. DeLongchamp, D.A. Fischer, E.K. Lin, L.J. Richter, M.L. Chabinyc, M.F. Toney, M. Heeney, I. McCulloch, Macromolecules 40 (2007) 7960–7965;
(b) D.M. DeLongchamp, R.J. Kline, E.K. Lin, D.A. Fischer, L.J. Richter, L.A. Lucas, M. Heeney, I. McCulloch, J.E. Northrup, Adv. Mater. 19 (2007) 833–837.
[23] M. Koppe, M. Scharber, C. Brabec, W. Duffy, M. Heeney, I. McCulloch, Adv. Funct. Mater. 17 (2007) 1371–1376.
[24] M.L. Chabinyc, M.F. Toney, R.J. Kline, I. McCulloch, M. Heeney, J. Am. Chem. Soc. 129 (2007) 3226–3237.
[25] (a) A.C. Mayer, M.F. Toney, S.R. Scully, J. Rivnay, C.J. Brabec, M. Scharber, M. Koppe, M. Heeney, I. McCulloch, M.D. McGehee, Adv. Funct. Mater. 19 (2009) 1173–1179;
(b) P.W.M. Blom, V.D. Mihailetchi, L.J.A. Koster, D.E. Markov, Adv. Mater. 19 (2007) 1551–1566.
[26] Y. He, Y. Li, Phys. Chem. Chem. Phys. 13 (2011) 1970–1983.
[27] (a) M.F. Falzon, M.M. Wienk, R.A.J. Janssen, J. Phys. Chem. C 115 (2011) 3178–3187;
(b) V.D. Mihailetchi, H. Xie, B. DeBoer, L.J.A. Koster, P.W.M. Blom, Adv. Funct. Mater. 16 (2006) 699–708;
(c) G. Zhao, Y. He, Z. Xu, J. Hou, M. Zhang, J. Min, H.-Y. Chen, M. Ye, Z. Hong, Y. Yang, Y. Li, Adv. Funct. Mater. 20 (2010) 1480–1487.
[28] K.S. Lee, K.Y. Yeon, K.H. Jung, S.K. Kim, J. Phys. Chem. A 112 (2008) 9312–9317.